Digest Journal of Nanomaterials and Biostructures Vol. 10, No. 2, April - June 2015, p. 663 - 680

MECHANISM OF ENHANCED HUMIC ACID REMOVAL FROM AQUEOUS SOLUTION USING POORLY CRYSTALLINE HYDROXYAPATITE NANOPARTICLES

W. WEI [a,b], L. YANG [a], W. ZHONG [a,b], J. CUI [a], Z. WEI [a,b*]
[a]*Jiangsu Provincial Key Laboratory of Materials Cycling and Pollution Control, Department of Environmental Science and Engineering, Nanjing Normal University, Nanjing 210023, China*
[b]*Jiangsu Center for Collaborative Innovation in Geographical Information Resource Development and Application, Nanjing 210023, China*

Poorly crystalline hydroxyapatite (HAP) nanoparticles synthesized by an improved neutralization method were used as novel adsorbents for removing humic acid (HA) from aqueous solution. Surface functionality, crystallinity, and morphology of the synthetic adsorbents were studied by FT-IR spectroscopy, powder X-ray diffraction and transmission electron microscopy. Characterization results showed that phase-pure, poorly crystalline and well dispersed HAP nanoparticles with average diameter of 30 nm were successfully obtained. Adsorption behaviors of HAP for HA were investigated by batch experiments and adsorption kinetic tests. HA adsorption process on the adsorbent obeyed pseudo-second-order kinetics and the adsorption rates decreased with increasing initial HA concentration. HA adsorption amount on the adsorbent decreased with increasing solution pH and the presence of alkali-earth metal ions resulted in the enhanced HA adsorption. HA adsorption on poorly crystalline HAP could be well described by Sips model and the maximum adsorption amount of the adsorbent for HA at 298 K was 123.44 mg/g. The FT-IR results revealed that HA adsorption over the adsorbent could be attributed to the surface complexation between the oxygen atoms of functional groups of HA and calcium ions of HAP. HA loaded adsorbent could be regenerated easily by using neutral phosphate buffer. Findings of the present work highlight the potential for using poorly crystalline HAP nanoparticles as effective and recyclable adsorbents for HA removal from aqueous solution.

(Received April 9, 2015; Accepted June 12, 2015)

Keywords: Humic acid, Poorly crystalline, Hydroxyapatite, Isotherm, Adsorption mechanism

1. Introduction

Humic substances (HS) are a complex mixture of compounds derived from the breakdown of plant and animal materials in the environment, corresponding to 50-80% of the natural organic matter (NOM) in water, soil and sediment [1]. Humic acid (HA) is one of the major components of HS and generally presents as dissolved organic matter in water [2]. It contains both hydrophobic and hydrophilic moieties as well as many organic functional groups such as carboxylic, phenolic, carbonyl, and hydroxyl groups connected with the aliphatic or aromatic carbons in the structure [3]. HA can bind various pollutants including synthetic organic chemicals (such as pesticides), and/or toxic heavy metals and carry them through water treatment facilities and distribution systems [4]. Furthermore, HA can be specifically targeted for removal from potable water supplies because they can adversely affect appearance and taste, and they can react with chlorine to form potentially carcinogenic chlorinated organic compounds [5]. Therefore, the presence of HA in water resources

*Corresponding author: weizhenggui@gmail.com

has been of major concerns in water supply and there is considerable practical interest to minimize the presence of humic acid in drinking water and other process waters [6].

To remove HA during water treatment, various approaches have been developed, such as chemical coagulation, membrane separation, advanced oxidation, ion exchange and adsorption [7-11]. Among them, Adsorption has been found to be superior to other techniques in terms of initial cost, flexibility and simplicity of design, ease of operation, insensitivity to toxic pollutants, and reduced production of secondary harmful substances [4,11]. Particularly, adsorption with activated carbon is considered to be one of the most economical and efficient methods for removing contaminants from water [12]. However, activated carbon is not very effective in removing macromolecules such as HA from water because its micropores are inaccessible for HA [2,13]. Therefore, the search for suitable adsorbents has led many researchers to explore more efficient techniques of using the natural and synthetic materials as adsorbents [13-22].

Recently, nanomaterials represent a promising application in a variety of fields due to their high surface area and reactivity and their ability to become dispersed in aqueous solution [23]. Nanomaterials usually exhibit higher reactivity and adsorption ability than the same material of normal size. In these regards, nanomaterials are the most promising candidates for pollutants removal from aqueous solution. Numerous attempts have been made to develop nanomaterial-based adsorbent for the removal of aqueous HA. For example, nanoporous carbon materials [13], nanoscale zero-valent iron [24], iron oxide magnetic nanoparticles [25], Mg/Al layered double hydroxides-Fe_3O_4 nanocomposites [26], magnetic chitosan nanoparticle [27], nanosized inorganic oxides (TiO_2, SiO_2, Al_2O_3, and ZnO) [28] and so on, have been used to eliminate aqueous HA because of their strong affinity for HA. However, most of these adsorbents suffer from high cost and/or the utilization of some environmentally incompatible additives. Therefore, the development of cheaper, more effective and biocompatible nanomaterial-based adsorbent is needed for HA removal.

Nanosized hydroxyapatite [$Ca_{10}(PO_4)_6(OH)_2$, HAP] possesses excellent biocompatibility and adsorption properties, and has been widely used as adsorbents for the adsorption and separation of biomolecules [29-31], and for the removal of heavy metals and phenol from contaminated soil and water [23,32-34]. The environmental risk of nanosized HAP itself can be neglected because it has displayed good cytocompatibility [35]. In our previpus work, nanosized HAP has been used as a biocompatible adsorbent for the adsorption of oxalic acid and fluoride [36,37], however, as to our knowledge, the adsorption and removal of HA by nanosized HAP has not been reported. Furthermore, little knowledge is available about the adsorption behaviors and influencing factors of HA onto nanosized HAP, and information concerning the interaction mechanisms of HA with poorly crystalline HAP is even more deficient. Considering that HAP can be used as an efficient adsorbent for removing phenol and low molecular weight organic acids that contain carboxylic group (such as acetic, oxalic, malic, and citric acids) from aqueous solution [20], HAP nanomaterial is expected to have a good affinity for HA in aqueous solution because HA contains phenolic and carboxylic groups.

In this study, HAP nanoparticles were prepared by an improved neutralization method and characterized by Fourier transform infrared (FTIR), powder X-ray diffraction (XRD), and transmission electron microscopy (TEM). The objective of this work was to investigate the potential candidate of poorly crystalline HAP as a new biocompatible adsorbent for the adsorption of HA from aqueous solution. The effects of adsorbent crystallinity, contact time, pH, ionic strength and the presence of alkali-earth metal ions were investigated by using batch experiments. The possible mechanisms for HA adsorption onto HAP were proposed.

2. Materials and methods

2.1 Materials

For the preparation of nanosized HAP, analytical grade $CaCO_3$ and H_3PO_4 were purchased from Shanghai Guoyao Chemical Company (China). HA was obtained as a commercial reagent-grade solid from Sigma (USA), and used without any further purification. All the other

chemicals used were of analytical grade.

2.2 Preparation and characterization of adsorbent

In the present work, nanosized HAP was prepared by a novel neutralization method with the assistance of ultrasonic irradiation. The neutralization method is chosen due to its simplicity and the fact that the reaction involves no foreign elements (the only by-product is water) [38]. However, it needs highly qualified and controlled parameters such as nature and composition of the starting materials, pH and temperature of the solutions prepared to obtain HAP nanoparticles. Sonochemistry represents a novel synthesizing method with a wide range of applications in the manufacture of nanomaterials. The transmission of ultrasound in a liquid phase provides mixing conditions favorable for chemical reaction, and generates transient extreme temperature or high shear-rate through acoustic cavitations, which has a specific effect on a chemical reaction that is very suitable for the formation of nanoparticles [39]. Ultrasonic irradiation has been used to prepare HAP and several other nanomaterials [40,41]. Briefly, the $Ca(OH)_2$ suspension was prepared by slurring CaO powder (obtained by calcination of $CaCO_3$ at 1100 °C for 24 h) into freshly double distilled water. The suspension was then exposed to an ultrasonic irradiation source of 50 W (30 kHz, Model UP50H, Hielscher Ultrasonics, Germany) at maximum amplitude for 1 h. Then a required amount of H_3PO_4 was added dropwise to $Ca(OH)_2$ suspension while undergoing a second hour of ultrasonic irradiation. During the synthesis process the Ca:P ratio was kept at 1.667. Intensive stirring and slow reagent addition were applied for the purpose of avoiding a local inhomogeneity. After complete addition, the resultant white slurry (pH = 7.0) was centrifuged at 10, 0000 ×g for 30 min. Then the precipitated HAP was washed with double distilled water and separated from the suspension by vacuum filtration. The resultant powders were dried at 80 °C for 24 h, and then calcined at 100 °C (denoted HAP-100), 400 °C (denoted HAP-400) and 800 °C (denoted HAP-800) for 4 h, respectively. The final products calcined at different temperatures were then characterized before being used in the batch adsorption studies.

The phase purity and crystallinity of the prepared HAP were determined by powder XRD using Cu Kα (λ=1.5405 Å) radiation on a Rigaku D/max-IIIB X-ray powder diffractometer. The morphology and size of the prepared HAP were characterized by a Hitachi Model H-7650 transmission electron microscope. The specific surface area of synthetic HAP was determined by nitrogen adsorption at 77 K (Micromeritics ASAP 2010). Surface area was calculated from adsorption data using BET equation. And batch equilibration technique [42] was applied to determine pH_{PZC} (point of zero charge) of prepared HAP. The FTIR spectra of HAP before and after the adsorption of HA were recorded on a Bruker Tensor 27 FTIR spectrometer (Bruker, Germany) with the KBr pellet technique.

2.3 Bath experiments

Bath adsorption studies were carried out by mixing certain amounts of HAP adsorbent with 100 mL of HA solution of varying concentration in a temperature-controlled air orbital shaker at 200 rpm with 250 mL stopper conical flasks. For the study on optimum pH, the initial pH values of HA solutions were varied from 3 to 10 by addition of drops of 0.1 mol/L NaOH or HNO_3 solutions. The conditions affecting HA adsorption onto nanosized HAP were studied by systematically varying the adsorbent crystallinity, contact time, pH, ionic strength and the presence of alkali-earth metal ions. The amount of HA in the solutions before and after adsorption was analyzed by ultraviolet visible spectrophotometer (UV-2450, Shimadzu) at a wavelength of 254 nm. The equilibrium adsorption capacity, q_e (mg/g) and removal rate, r (% removal), are expressed as follows: $q_e = (C_0 - C_e)V/m$ and $r = (C_0 - C_e)/C_0$, where C_0 and C_e are the initial and equilibrium concentrations of HA (mg/L) in solution; V (L) is the volume of aqueous solution containing HA; and m (g) is the weight of adsorbent. All adsorption experiments were conducted in triplicates and the results were reported as average. The relative deviations met with the requirement of less than 5%.

2.4 Mathematical models

The adsorption kinetics of HA on HAP nanoparticles were described with the pseudo-first-order equation (1) [43] and pseudo-second-order equation (2) [44], respectively:

$$q_t = q_e(1 - \exp(-k_1 t)) \quad (1)$$

$$q_t = \frac{q_e^2 k_2 t}{1 + q_e k_2 t} \quad (2)$$

where k_1 (1/min) and k_2 (g/(mg·min)) are the rate constants for the pseudo-first-order and pseudo-second-order models, respectively; q_e (mg/g) is the amount of adsorbate adsorbed per unit adsorbent at equilibrium. Herein, the initial adsorption rate (v_0) is calculated as: $v_0 = k_2 q_e^2$ for the pseudo-second-order model.

Langmuir (4) [45], Freundlich (5) [46] and Sips isotherm models (6) [47] were used to describe the adsorption of HA on the HAP nanoparticles:

$$q_e = \frac{q_m K_L C_e}{1 + K_L C_e} \quad (4)$$

$$q_e = K_F C_e^{1/n} \quad (5)$$

$$q_e = \frac{q_m (K_S C_e)^{1/n}}{1 + (K_S C_e)^{1/n}} \quad (6)$$

where K_L (L/mg), K_F [mg/g(L/mg)$^{1/n}$] and K_S (L/mg) are the equilibrium constants of Langmuir, Freundlich and Sips models, respectively; q_e(mg/g) is the adsorption capacity at equilibrium; C_e (mg/L) is the equilibrium concentration of HA in solution; q_m (mg/g) is the maximum adsorption capacity, and 1/*n* is the heterogeneity factor.

2.5. Desorption and regeneration studies

To evaluate the reusability of the nanosized HAP adsorbent, adsorption of HA and regeneration of HA-loaded adsorbent were performed in four consecutive cycles. In each cycle, 80 mg/L HA in 100 mL of solution was mixed with 200 mg nanosized HAP for 24 h. After achieving the adsorption equilibrium, HA loaded nanosized HAP was centrifuged and the residual HA concentration was detected spectrometrically. HA loaded nanosized HAP was redispensed in 0.5 mol/L KH_2PO_4 solution and shaken for 1 h. Then the suspension was centrifuged and the solid residues were used again in the subsequent experiments for the adsorption of HA.

3. Results and discussions

3.1 Characterization of the synthesized nanosized HAP

Fig. 1 showed the XRD patterns of the synthesized HAP calcined at the different temperatures for 4 h. All the samples were in good agreement with the reference pattern of pure HAP (JCPDS no. 09-0432). It could be seen that there were numerous sharp peaks and low background in the XRD pattern of the HAP samples. Meanwhile, the XRD pattern of the samples did not reveal any other phases than HAP. However, the degrees of crystallinity of HAP-100, HAP-400, and HAP-800 were different. For HAP-800, (calcined at 800 °C), many sharp peaks appeared, suggesting that the sample was well crystalline. By contrast, the broad peaks of the XRD pattern of HAP-100 indicated that the particles were very small and poorly crystalline. From XRD data, the fraction of the crystalline phase (X_c) in HAP samples could be determined as: $X_c = 1 - (V_{112/300}/I_{300})$, where $V_{112/300}$ represented the intensity of the hollow between diffraction peaks (112) and (300), and I_{300} was the

intensity of (300) diffraction peak [48]. The crystallinity of HAP-100, HAP-400 and HAP-800 were 0.28, 0.62 and 0.85, respectively. The average particle size (*D*) of the synthetic HAP samples could be calculated from the XRD line broadening measurement from the Scherrer formula [49]: $D = 0.89\lambda/\beta\cos\theta$, where λ is the X-ray wavelength (1.5405 Å), β is the full width at the half maximum of the HAP (211) line and θ is the diffraction angle. The average particle sizes of HAP-100, HAP-400 and HAP-800 were 30, 61 and 122 nm, respectively. It was clear to see that increasing the calcining temperature resulted in the larger particle size and higher crystallinity.

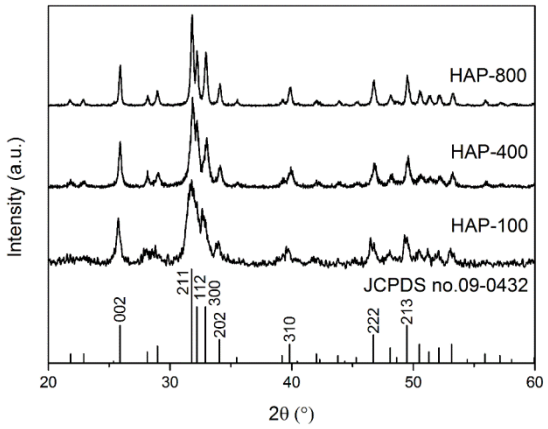

Fig.1. The XRD patterns of the synthetic nanosized HAP calcined at 100 °C (HAP-100), 400 °C (HAP-400), and 800 °C (HAP-800), and the reference pattern of pure HAP (JCPDS no. 09-0432).

The TEM micrographs of the HAP particles calcined at different temperatures were shown in Fig. 2. All the synthetic HAP samples showed nanosized particles ranging from needle-like structures to spherical particles. The particle size of the HAP samples were distributed in the range of 30-120 nm, which was in consistent with the XRD data. The results also showed that increasing the calcining temperatures resulted in the higher aggregation and larger particle size, which would decrease the specific surface area, and thus ultimately reduced the adsorption capacity of HA on HAP nanoparticles.

The surface area of HAP-100, HAP-400 and HAP-800 measured by the BET method were determined to be 72.1, 48.6, and 24.2 m^2/g, respectively. The pH_{PZC} is a concept related to the phenomenon of adsorption that describes the condition when the electrical charge density on the adsorbent surface is zero. The pH_{PZC} were found to be 7.2, 7.5 and 7.7, for HAP-100, HAP-400 and HAP-800, respectively.

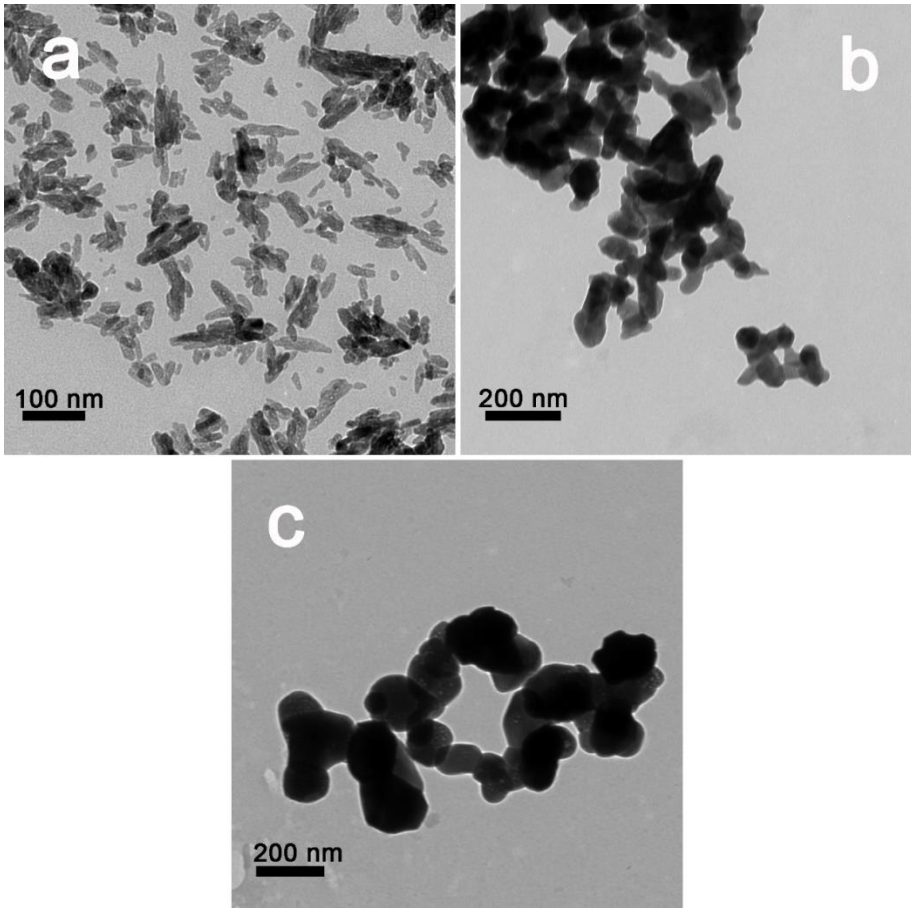

Fig.2. The TEM micrographs of the synthetic prepared HAP with different crystallinity. (a) X_c= 0.28, calcined at 100 °C; (b) X_c= 0.62, calcined at 400 °C; (c) X_c= 0.85, calcined at 800 °C.

3.2 Effect of crystallinity on HA adsorption

Fig. 3 showed the effect of crystallinity on HA adsorption onto nanosized HAP adsorbents. It was clear to see that the adsorption capacity decreased with increasing crystallinity. With the increase in HAP crystallinity from 0.28 to 0.62, the HA adsorption capacity and removal rate decreased rapidly from 53.92 to 49.05 mg/g, and 77.0 to 70.1% (140 mg/L HA), respectively. With a further increase in HAP crystallinity to 0.85, the HA adsorption capacity and removal rate decreased remarkably 43.12 mg/g, and 61.5% (140 mg/L HA), respectively. The decrease of the adsorption ability was attributed to the increase of the particle size and crystallinity of HAP after calcining at high temperatures. It was generally accepted that the adsorption ability of HAP was controlled by the surface area, which showed a direct dependence on the particle size and crystallinity of HAP. Da Rocha et al.[50] have indicated that the drop in the adsorption capacity of HAP for cadmium could be explained by a reduction in its surface area, which was induced by the increase of the crystallinity and particle size. In another work, we had revealed previously the crystallinity-dependent defluoridation properties of nanosized HAP, that the poorly crystalline apatite materials derived from lower calcining temperature exhibited higher adsorption capacity for fluoride than those from higher calcining temperature [51]. Therefore, it could be concluded that the decrease in crystallinity of HAP led to an increase in surface area, accompanied by a concomitant rise in the quantity of active sites on the surface, which would cause a remarkable enhancement of the adsorption ability. And thus the adsorption ability for HA of the poorly crystalline HAP-100 was much higher than that of HAP-400 and HAP-800, indicating that the poorly crystalline HAP-100 was more suitable as an efficient adsorbent for removing HA from aqueous solution. In this study, HAP-100 was chosen as adsorbent for the removal of HA.

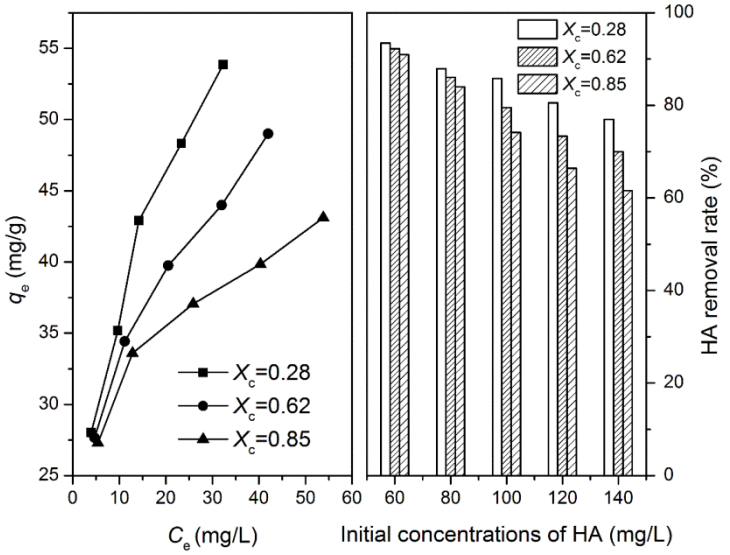

Fig.3. Effect of crystallinity on HA adsorption. (adsorption conditions: adsorbent dosage = 2 g/L, initial pH 8.0, and temperature = 298 K).

3.3 Effect of pH on HA adsorption

The most critical parameter affecting the adsorption process in the removal of HA by the nanosized HAP is the pH of the adsorption medium. This is due to the charge of the adsorbate and the adsorbent often depending on the pH of the solution. The adsorption of HA onto poorly crystalline HAP-100 (hereafter HAP) was studied at different initial pH between 3 and 10. Fig. 4 (left panel) showed that an increase in solution pH from 3 to 10 caused an obvious decrease in the HA adsorption capacity for poorly crystalline HAP from 39.61 to 35.04 mg/g (80 mg/L HA), 49.24 to 40.65 mg/g (100 mg/L HA), and 58.93 to 44.71 mg/g (120 mg/L HA), respectively. This indicated that the adsorption of HA on poorly crystalline HAP was favored at lower pH value.

It was generally accepted that the HA could be considered as a mixture of compounds with weakly acidic functional groups, such as carboxylic and phenolic groups [2]. Since the pK_a values of carboxyl and phenolic groups were around 3.0 and 9.0, HA was expected to be negatively charged by deprotonation of carboxylic groups at pH above 3.0 [20,21]. For poorly crystalline HAP, it has been reported that HAP exhibited amphoteric properties, and acted as a buffer in a wide pH range from 4.0 to 10.0 [42], similar results were obtained as shown in the right panel of Fig. 4. The buffering characteristics and surface charge of HAP were expected to be the result of acid-base interactions of the reactive surface sites [52]. The pH_{PZC} of the poorly crystalline HAP was determined to be 7.2. Below the pH_{PZC} of HAP, protons in the solution were consumed by the protonation of the surface $\equiv PO^-$ and $\equiv CaOH$ groups, resulting in the increase of final pH value [53]. While the positively charged $\equiv CaOH_2^+$ and neutral $\equiv POH$ sites prevailed on HAP surface, making surface charge of HAP positive in this pH region. And thus the adsorption of HA onto HAP might be achieved through the electrostatic attraction between the negatively charged HA molecules and the positively charged HAP surface. Similar findings have been reported by Zhan et al. [20]. In addition, below pH_{PZC}, the overall HAP surface was positively charged and the oxygen atom of functional groups of HA might interact via Lewis acid-base interactions with Ca^{2+} groups of HAP [54]. Furthermore, the adsorption of HA on HAP at pH below the pH_{PZC} might also be achieved through hydrogen bonding. For example, the $\equiv POH$ groups on the HAP surface and the carboxylic, phenolic hydroxyl groups of HA molecules might form hydrogen bonding [20]. Our previous study [55] have also indicated that carboxylic groups of organic acids might interact via hydrogen bonding with $\equiv POH$ on nanosized HAP. On the other hand, in the range of higher initial pH values (above pH_{PZC}), OH^- could be consumed by deprotonation of surface $\equiv CaOH_2^+$ and $\equiv POH$ sites and thus

final pH decreased (Fig. 4, right panel). Consequently, neutral ≡CaOH and negatively charged ≡PO^- species predominated in alkaline solutions, causing HAP surface to become negatively charged in alkaline solutions [53]. In this case, increasing pH might result in increased electrostatic repulsive force between the negatively charged HA molecules and the negatively charged HAP surface, which might decrease the HA adsorption on HAP. However, despite the electrostatic repulsion a considerable amount of HA was adsorbed by poorly crystalline HAP. This suggested other mechanisms such as hydrogen bonding and Lewis acid-base interaction might be involved in the HA adsorption by HAP at higher pH values. For example, the ≡PO^- groups on the HAP surface and the phenolic hydroxyl groups of HA molecules might form hydrogen bonding [20, 54]. While the adsorption of HA on HAP at pH above the pH_{PZC} of HAP might be also attributed to the Lewis acid-base interaction between the oxygen atom of functional groups of HA and the Ca^{2+} groups of HAP. Furthermore, it was notable that HA molecular size might increase from a spherical structure at low pH to a linear or stretched structure at high pH, which also accounted for the reduced HA adsorption at increased pH [11].

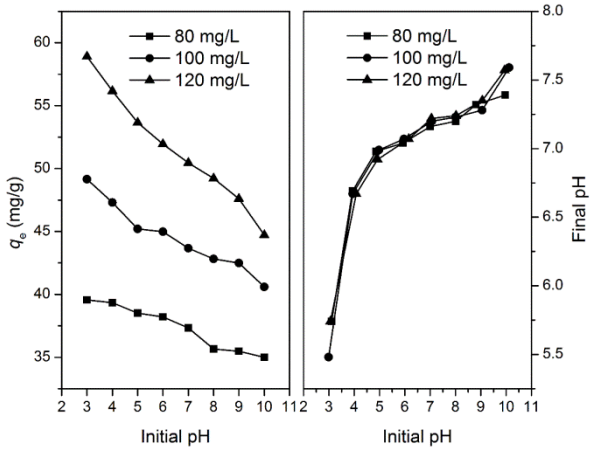

Fig.4. Effect of pH on the adsorption of HA onto poorly crystalline HAP (adsorption conditions: adsorbent dosage = 2 g/L, temperature = 298 K).

3.4 Effect of adsorbent dosage on HA adsorption

The effect of adsorbent dosage on the adsorption of HA on poorly crystalline HAP was shown in Fig. 5. It indicated that an increase in adsorbent dosage from 0.2 to 3 g/L resulted in the increase of HA removal efficiency from 40.4 to 97.4%, 37.1 to 97.1%, 34.2 to 94.0% and 28.1 to 90.6%, for 40, 60, 80 and 100 mg/L, respectively. The increase in HA removal rate with increasing adsorbent dosage was due to the increase in the adsorbent concentration, which increased the available surface area and adsorption sites. However, the HA adsorption capacities for HAP decreased with increasing adsorbent dosage (Fig. 5, left panel). This was attributed to a split in the flux or the concentration gradient between the HA concentration in the solution and the HA concentration in the adsorbent surface, resulting in that the amount of HA adsorbed onto unit weight of adsorbent gets reduced with increasing adsorbent dosage [2]. In other words, the decrease in adsorption capacity with the increase in the adsorbent dosage was mainly attributed to the unsaturation of the adsorption sites through the adsorption process. Similar findings have been observed for HA removal by surfactant-modified chitosan/zeolite composite [2] and surfactant modified zeolite [4], as well as for phenol [33] and fluoride [51] removal by HAP nanoparticles.

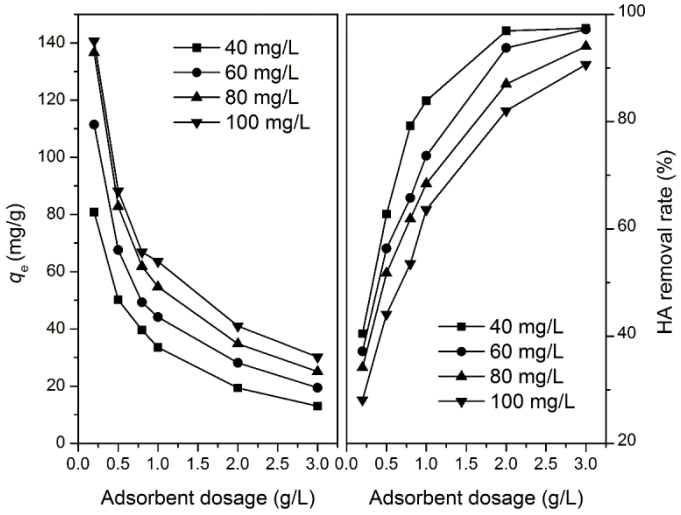

Fig.5. Effect of adsorbent dosage on HA adsorption by poorly crystalline HAP (adsorption conditions: adsorbent dosage = 2 g/L, initial pH 8.0, and temperature = 298 K).

3.5 Effect of contact time on HA adsorption and adsorption kinetics

The effect of contact time on adsorption of HA on HAP was carried out at 2-1440 min as shown in Fig. 6. Results showed that the adsorption of HA by HAP took place in two distinct steps: a relatively fast phase (first 60 min), followed by a slow increase until the state of equilibrium was reached. It was obvious that the rate of HA adsorption was rapid initially with more than 70% of HA was able to be adsorbed within 60 min for the initial HA concentrations of 20, 40 and 80 mg/L. The necessary time to reach the equilibrium was about 24 h, thereafter, no detectable concentration changes occurred and the average removal rate of HA reached about 98.6% (9.86 mg/g adsorption capacity), 96.7% (19.28 mg/g adsorption capacity), 89.9%(35.33 mg/g adsorption capacity), and 81.1%(48.66 mg/g adsorption capacity) when the initial concentrations of HA were 20, 40, 80 and 120 mg/L, respectively. The initial rapid phase (during the first 60 min of adsorption) was due to the availability of adsorption sites for the adsorption of HA, while the second slower phase was due to the quick exhaustion of the adsorption sites [56].

To investigate the mechanism of HA adsorption on adsorbents, the pseudo-first-order model and pseudo-second-order model were used to fit the adsorption kinetics data. Adsorption kinetics parameters calculated from the pseudo-first-order and pseudo-second-order kinetics were listed in Table 1. As shown in Table 1, the correlation coefficients (R^2) of pseudo-second-order kinetics were greater than the pseudo-first-order kinetics and the calculated q_e agreed much better with the experimental data than that of pseudo-first-order kinetics, which suggested that HA adsorption on HAP could be better fitted by the pseudo-second-order kinetic model based on the assumption that the rate determining step might be chemisorption between adsorbent and adsorbate. The results in Table 1 also illustrated that both the rate constants k_1 and k_2 decreased with increasing initial HA concentrations, which revealed the fact that it was faster for an adsorption system with HA at lower initial concentrations to reach equilibrium. The presence of higher adsorption rates at lower HA concentrations and lower adsorption rates at higher HA concentrations has been extensively reported for HA removal by several other adsorbents, such as surfactant-modified chitosan/zeolite composite [2], polyaniline/attapulgite composite [11], surfactant-modified hydroxyapatite/zeolite composite [20], and magnetically separable polyaniline [57].

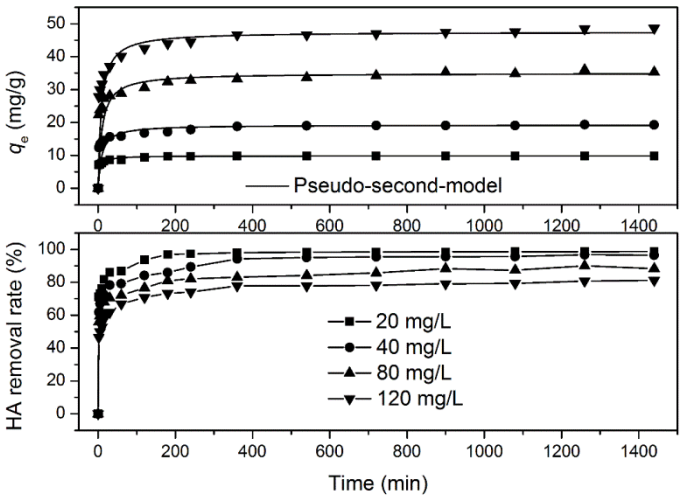

Fig.6. Adsorption kinetics of HA on poorly crystalline HAP at different initial concentrations (adsorption conditions: adsorbent dosage = 2 g/L, initial pH 8.0, and temperature = 298 K).

Table 1 Pseudo-first-order model and pseudo-second-order kinetic model constants for HA adsorption on poorly crystalline HAP at different initial HA concentrations.

C_0 (mg/L)	q_e, exp (mg/g)	Pseudo-first-order model			Pseudo-second-order model		
		q_e, cal (mg/g)	k_1 (1/min)	R^2	q_e, cal (mg/g)	k_2 (g/(mg·min))	R^2
20	9.864	1.777	6.43×10^{-3}	0.8431	9.890	2.59×10^{-2}	0.9999
40	19.284	5.415	4.64×10^{-3}	0.8665	19.253	5.77×10^{-3}	0.9995
80	35.327	10.752	3.33×10^{-3}	0.7984	34.990	2.96×10^{-3}	0.9991
120	48.661	14.506	3.12×10^{-3}	0.7627	47.551	2.48×10^{-3}	0.9997

3.6 Effects of ionic strength and alkali-earth metal ions on HA adsorption

The adsorption of HA onto poorly crystalline HAP might be affected by the presence of inorganic salts. In this study, the ionic strength of the solutions was adjusted with the use of KNO_3. Based on the results shown in Fig. 7 (left panel), it was evident that HA adsorption amount onto HAP increased with the increasing ionic concentration of KNO_3 at ionic concentration from 0 to 2 mmol/L. When HA initial concentration was 140 mg/L, the adsorption capability increased from 53.86 mg/g (0 mmol/L KNO_3) to 57.06 mg/g (1 mmol/L KNO_3) and 66.12 mg/g (2 mmol/L KNO_3), respectively. Similar observations were found for HA adsorption on fly ash derived carbon [58] and hematite [59]. In addition, the alkaline-earth metal ions Ca^{2+} and Mg^{2+} are frequently found in natural water, which might interact with HA molecules, therefore affect the HA adsorption on the adsorbent [15]. Effect of Ca^{2+} and Mg^{2+} on the adsorption of HA by poorly crystalline HAP was illustrated in Fig. 7 (right panel). Based on the plots, HA adsorption amount onto HAP increased with the increasing ionic concentration of Ca^{2+} and Mg^{2+} at ionic concentration from 0 to 0.2

mmol/L. For the HA solution of 140 mg/L, the presence of alkaline-earth metal ions resulted in an increase in HA adsorption capacity from 53.86 mg/g (0 mmol/L alkaline-earth metal ions) to 59.27 mg/g (0.1 mmol/L Mg^{2+}), 64.26 mg/g (0.2 mmol/L Mg^{2+}), and 61.93 mg/g (0.1 mmol/L Ca^{2+}), 68.57 mg/g (0.2 mmol/L Ca^{2+}), respectively.

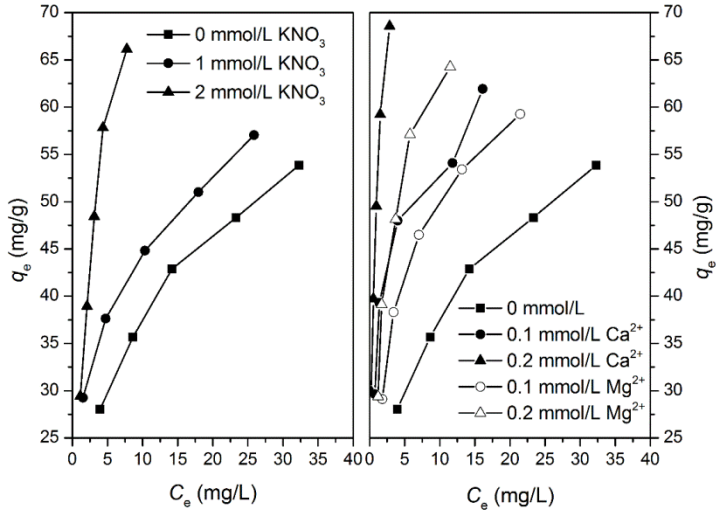

Fig.7. Effects of ionic strength (left panel) and alkali-earth metal ions (right panel) on the adsorption of HA by poorly crystalline HAP (adsorption conditions: adsorbent dosage = 2 g/L, initial pH 8.0, and temperature = 298 K).

The effects of ionic strength and alkali-earth metal ions on HA adsorption could be attributed to several mechanisms [11,15,17,60,61]: (1) The increase of ionic strength, which resulted in minimization of the electrostatic repulsion between ionized oxygen groups and decreased molecular volume of HA, facilitated the adsorption. (2) An increase in ionic strength caused HA to become more coiled and more compact, allowing more HA to occupy the same surface area of HAP. (3) At high ionic strength HA diffused faster due to its coiled structure. (4) An increase in ionic strength caused the compression of the thickness of the diffuse double layer which surrounded solid and liquid phases when they were in contact. Such compression helped the adsorbent and HA molecules to approach each other more closely. (5) The presence of K^{+}, Ca^{2+} and Mg^{2+} might weaken the repulsive interaction between HA molecules bounded to the surface of the adsorbents and HA molecules in solution. (6) Bridging of Ca^{2+} and Mg^{2+} between HA molecules and hydroxyl group on the HAP surface could enhance the adsorption of HA. Furthermore, as shown in Fig. 7 (right panel), the enhancement of HA adsorption by Ca^{2+} was greater than that of Mg^{2+}. This might be due to that Ca^{2+} ions had larger ionic size and larger equilibrium formation constant with HA relative to Mg^{2+} ions, thus interacting more strongly with HA molecules. And this could lead to a larger amount of HA adsorbing onto the same surface area of poorly crystalline HAP in the presence of Ca^{2+} ions than Mg^{2+} ions [62].

3.7 Adsorption isotherms

Adsorption isotherms describe the distribution of adsorbate between adsorbent and solution when adsorption process reaches the equilibrium, which are important data to elucidate the adsorption mechanism. In this study, the adsorption isotherms of HA on poorly crystalline HAP were obtained at different pH values, ranging between 4 and 8, at 298 K. As shown in Fig. 8, the adsorption amounts of HA on HAP increased sharply with the increasing HA concentration in the initial stages, which indicated that there were numerous readily accessible sites. Moreover, the results also indicated that the amount of adsorption increased by decreasing the pH of solution.

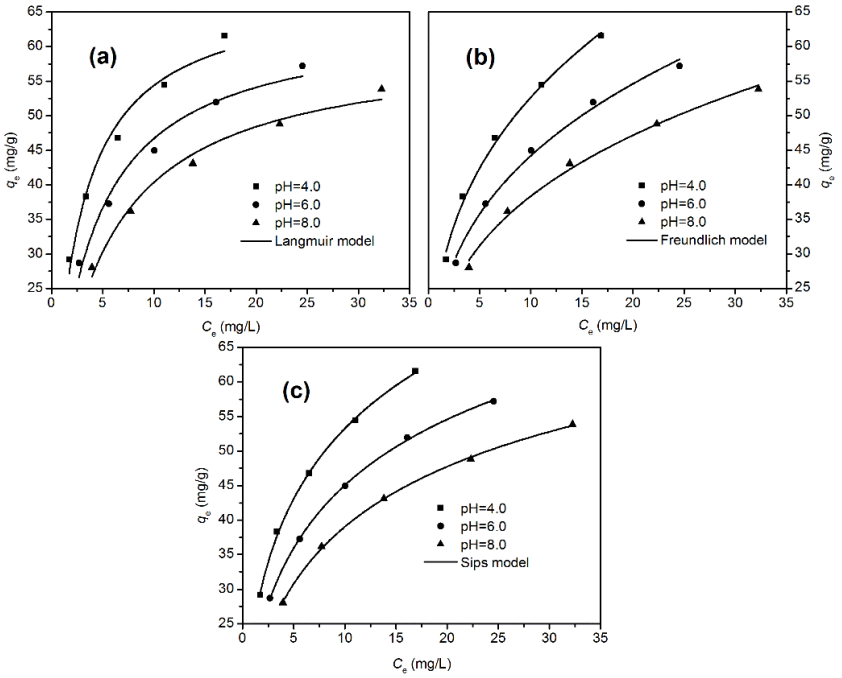

Fig.8. Non-linear Langmuir (a), Freundlich (b), and Sips (c) isotherms at different pH values for the adsorption of HA onto poorly crystalline HAP (adsorption conditions: adsorbent dosage = 2 g/L, initial pH 8.0, and temperature = 298 K).

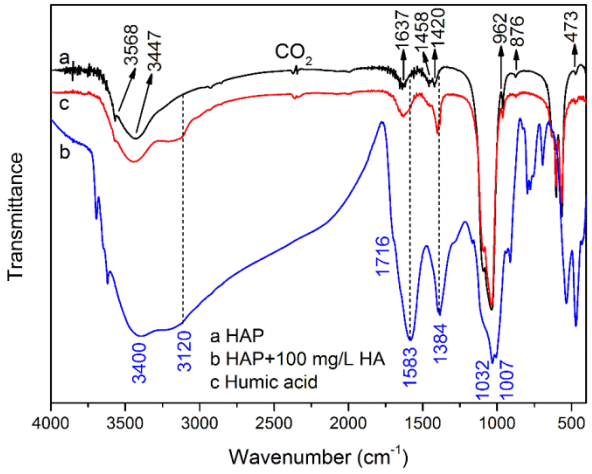

Fig.9. The FT-IR spectra of HAP (a), HA (b), and HA loaded HAP.

The adsorption isotherm experimental data collected at different HA concentrations and various pH values were fitted with three common adsorption models: Langmuir, Freundlich, and Sips (also known as Langmuir-Freundlich) isotherm models. In all cases, the Levenberg-Marquardt method was used in order to determine the fitting parameters. The Langmuir isotherm model assumes that the adsorption takes place at specific homogenous sites within the adsorbent and is commonly used for monolayer adsorption [45]. Unlike the Langmuir model, the Freundlich isotherm model is an empirical equation and the model is valid for heterogeneous surfaces. It assumes that the adsorption process occurs on the heterogeneous surfaces and the adsorption capacity is related to the concentration of HA at equilibrium [46]. While the Sips isotherm model could be considered as a combination of Langmuir and Freundlich equations [47].

The fitting parameters for HA adsorption isotherms based on Langmuir, Freundlich and Sips

equations were listed in Table 2. The Freundlich and Sips models gave much better fit to the experimental data compared to that of the Langmuir isotherm model, revealing that the adsorption of HA on poorly crystalline HAP was multilayer adsorption rather than monolayer coverage. Because the HAP surface was heterogeneous with "C" and "P" sites [63], thus violating the assumption of the Langmuir isotherm equation. From the non-linear plots of the Freundlich isotherm, the values of K_F were 25.64, 21.89 and 19.30 [mg/g(L/mg)$^{1/n}$] at pH 4.0, 6.0 and 8.0, respectively. K_F values increased continuously as the pH was increased. This suggested that at lower pH, the heterogeneous adsorption sites played a more important role thus contributing to multilayer adsorption. In addition, 1/*n* values lied between 0.1 and 1 for different pH values, suggesting the HAP was favorable for adsorption of HA under conditions used in this study. Moreover, the Freundlich exponent 1/*n* between 0.2984 and 0.3126 indicated a high affinity of HAP for HA and the great heterogeneity of HAP surface.

The comparison of the three adsorption models (Fig. 8 (a, b, c)) showed that the Sips model provided the best fit with the experimental results. Based on Table 2, all 1/*n* values obtained were less than 1, indicating that the poorly crystalline HAP was a heterogeneous adsorbent for the adsorption of HA. As the pH decreased, the 1/n value became much less than one and this indicated the presence of more heterogeneous binding sites. This observation agreed with the Freundlich isotherms analyses. Based on the Sips isotherm model, the predicted maximum capacity of adsorbent, q_m, was found to be 123.44, 103.80, and 90.70 mg/g at pH 4.0, 6.0 and 8.0, respectively. It is also important to compare the value of maximum adsorption capacity obtained from this study with values from other reported adsorbents, since this will suggest the effectiveness of poorly crystalline HAP as a potential adsorbent for treatment of water containing HA. The adsorption capacity for HA using poorly crystalline HAP is comparable with other reported adsorbents as shown in Table 3.

Table 2 Parameters of adsorption isotherms of HA on poorly crystalline HAP at different pH values (298 K).

Initial solution pH	Langmuir model			Freundlich model			Sips model			
	q_m (mg/g)	K_L (L/mg)	R^2	K_F [mg/g (L/mg)$^{1/n}$]	1/*n*	R^2	q_m (mg/g)	K_S (L/mg)	1/n	R^2
4.0	68.47	0.386	0.9700	25.64	0.3126	0.9945	123.44	0.05772	0.5010	0.9984
6.0	64.29	0.265	0.9721	21.89	0.3054	0.9927	103.80	0.06071	0.5320	0.9992
8.0	60.48	0.200	0.9791	19.30	0.2984	0.9922	90.70	0.06046	0.5562	0.9991

Table 3 The comparison of maximum HA adsorption capacities of various adsorbents on the basis of Langmuir isotherm model.

Adsorbent	q_m (mg/g)	Equilibrium time (h)	Adsorbent dosage (g/L)	pH	Temperature (*K*)	References
CSZ	74.1	24	1.0	7.0	303	[2]
SMCSZ	164	24	1.0	7.0	303	[2]
SMZFA L	31.6	24	5.0	NA*	293	[4]
SMZFA F	126.6	24	5.0	NA	293	[4]
Chitosan-ECH beads	44.84	1	0.5	6.0	280	[10]
ATP-PANI	52.91	24	0.5	5.0	298	[11]
RHA-NH_2	8.2	1	5.0	6.0	298	[14]
MS-PEI	128.64	20	0.2332	6.96	298	[18]
APTS-SBA-15-5%	72.5	24	0.4	7.0	298	[21]
MCNP	32.6	1	1.0	7.0	298	[27]
Unburned carbon	71.8	200	0.5	7.0	303	[58]
Activated bentonite	10.81	5	12	NA	308	[61]
Poorly crystalline HAP	60.48	24	2.0	8.0	298	This study

* NA: not available.

3.8 FTIR spectroscopic analysis

Further information about the interaction of HA with HAP was garnered by the FTIR spectra data (Fig. 9). The prepared poorly crystalline HAP (spectrum a) showed characteristic bands forPO_4^{3-}(473, 565, 603, 962, 1043 and 1092 cm^{-1}), OH^- (629 and 3568 cm^{-1}), and adsorbed water (1637 and 3447 cm^{-1}), which indicated that the synthetic sample was pure HAP [55]. Some carbonate derived bands were observed at 876 cm^{-1} and around 1420 and1458 cm^{-1}. It might be due to the adsorption of atmospheric car-bon dioxide during the sample preparation. This small amount of carbonate has not produced either carbonate substituted HAP (as evident by XRD) or other carbonates [64]. A number of absorption peaks were shown in spectrum b of Fig. 9, indicating the presence of different types of functional groups for the HA. A strong and wide band appeared around 3400 cm^{-1} was assigned to the -OH stretch of various hydroxylated functional groups, while a shoulder at 1716 cm^{-1} attributed to C=O stretching of COOH and ketones, and a strong peak at 1583 cm^{-1} associated to structural vibrations of aromatic C=C and asymmetrical C=O stretching of COO^- groups [65]. The medium intensity absorption centered 1384 cm^{-1}, mostly due to the symmetrical COO- stretching. The peaks at 1032 and 1007 cm^{-1} indicated C-O stretching of polysaccharides or polysaccharide-like substances, or Si-O of silicate impurities [66]. A number of additional peaks above 3500 cm^{-1} and below 1100 cm^{-1} were apparent in the spectrum of HA. These bands might be attributed to alcoholic and polysaccharide C-O stretch and/or to Si-O vibrations of clay impurities in HA samples [67].

In order to understand the changes of FTIR spectra after HA adsorption on HAP and elucidate the mechanism of HA adsorption on HAP, the the FTIR spectrum of HA loaded HAP were characterized and shown in spectrum c of Fig. 9. Compared the FT-IR spectrum of HA loaded HAP with pristine HAP, some differences could be observed. The 3120 cm^{-1} feature was assigned to -OH stretching vibrations associated with waters tightly associated with the HA bound calcium. In addition, the peaks of 1716 and 1583 cm^{-1} were completely disappeared and the band around 1637 cm^{-1} became higher. It was considered that since the 1716 and 1583 cm^{-1} have essentially disappeared in HA loaded HAP spectra, and since the new peaks (around 1637 cm^{-1}) were consistent with a -COO-metal asymmetric stretch, the data provided clear evidence that carboxylic groups of HA were deprotonated by the complexation with HAP surface species ($\equiv CaOH_2^+$, $\equiv CaOH$).

3.9 Desorption and regeneration

The economic efficiency and environmental sustainability should be taken into account during the process of wastewater treatment. A desorption study will help to elucidate the nature of adsorption process and to reuse the adsorbent [10]. Several desorbing reagents have been reported for desorption of HA from various adsorbents, such as NaOH, HCl, NaCl, NaAc, $NaCO_3$ and $NaHCO_3$ [10,11,18,60,68]. It was generally found that the desorption efficiency of HCl and NaOH was greater than that of the other desorption reagents. However, the acidic agents could not be used for desorption of HA from HAP since solubility of HAP in aqueous media increased with lowering pH value [55]. Furthermore, although NaOH has been widely used to desorb HA successfully [11,18,60], it was found that, only 3% of the adsorbed HA was desorbed from poorly crystalline HAP by 2 mol/L NaOH (data not shown). This phenomenon was mainly due to strong chemical adsorption, suggesting that the immobilization of HA on HAP was high affinity interaction through complexation. Alternatively, phosphate buffer including considerably weak acids $H_2PO_4^-$ and HPO_4^{2-} was expected to desorb HA from HAP. It was considered that these phosphate ions had the ability to disturb adsorption of HA molecules on the HAP surface, and to bind strongly to Ca^{2+} of HAP [69]. Therefore, attempts were made to desorb HA from HA-loaded HAP using 0.5 mol/L KH_2PO_4 solution. Results showed that the desorption efficiency of HA from HA-loaded HAP was found to be 92.5% at the first cycle. The regenerated HAP samples were reused for four consecutive cycles. Fig. 10 showed the recycling of HAP in the removal of HA. Only a slight loss in adsorption capacity was observed after four cycles of consecutive adsorption-desorption, demonstrating that poorly crystalline HAP was high-performance recyclable adsorbent for the removal of HA.

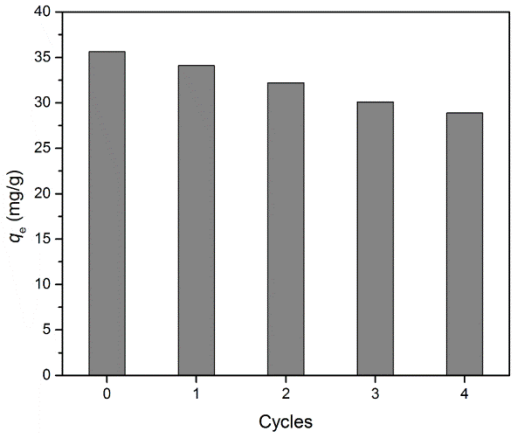

Fig.10. HA adsorption on virgin and regenerated poorly crystalline HAP adsorbent with four adsorption-regeneration cycles. (adsorption conditions: adsorbent dosage = 2 g/L, initial pH 8.0, initial HA concentration = 80 mg/L, and temperature = 298 K)

4. Conclusions

In this study, the poorly crystalline HAP was prepared by an improved neutralization method and used as an adsorbent to remove HA in aqueous solution. Adsorption batch experiments indicated the poorly crystalline HAP exhibited considerable superiority to those well crystalline HAP for HA adsorption in terms of adsorption capacity. The HA adsorption capacities for HAP decreased with increasing solution pH from 3 to 10. Increasing the adsorbent dosage increased the number of adsorption sites and further enhanced the removal rate of HA, but decreased the specific adsorption capacity. The presence of alkali-earth metal ions improved HA adsorption on the adsorbents. Adsorption isotherms of HA on the adsorbent could be fitted by Sips model and HA adsorption process follows pseudo-second-order kinetics. HA loaded adsorbent could be desorbed in phosphate solution and the regenerated adsorbent still possessed high adsorption capacity for HA. Lewis acid-base interaction (surface complexation), electrostatic interaction, and hydrogen bonding were inferred to be the main mechanisms of adsorption of HA on HAP. The present findings highlighted that the poorly crystalline HAP nanoparticles possessed great potential for effective removal of HA in water treatment.

Acknowledgements

This work is supported by the National Natural Science Foundation of China (No. 41303081), the National Programs for High Technology Research and Development of China (No. 2007AA10Z406), the Research Fund for the Doctoral Program of Higher Education (Nos. 20113207110014and 20133207120019), the Foundation for Talent Recommendation Program of Nanjing Normal University (Nos. 2009103XGQ0063 and 2011105XGQ0247), SRF for ROCS, SEM, and PAPD (a project funded by the Priority Academic Program Development of Jiangsu Higher Education Institutions (NO. 164320H116).

References

[1] G. Abate, J.C. Masini, Colloids Surf. A **226**, 25 (2003).
[2] J.W. Lin, Y.H. Zhan, Chem. Eng. J. **200-202**, 202 (2012).
[3] K. Ghosh, M. Schnitzer, Soil Sci. **129**, 266 (1980).
[4] C.J. Li, Y. Dong, D.Y. Wu, L.C. Peng, H.N. Kong, Appl. Clay Sci. **52**, 353 (2011).

[5] K. Satoshi, I. Kumiko, K. Hideyuki, S. Tohru, M. Kazuaki, F. Kunihiro, H.Kazuyuki, O. Kiyohisa, Environ. Sci. Technol. **37**, 1448 (2003).
[6] X. Zhang, R. Bai, J. Colloid Interface Sci. **264**, 30 (2003).
[7] B. Bolto, D. Dixon, R. Eldridge, S. King, K. Linge, Water Res. **36**, 5057 (2002).
[8] J. Cho, G. Amy, J. Pellegrino, J. Membr. Sci. **164**, 89 (2000).
[9] C. Volk, K. Bell, E. Ibrahim, D. Verges, G. Amy, M. LeChevallier, Water Res. **34**, 3247 (2000).
[10] W.S. Wan Ngah, M.A. Hanafiah, S.S. Yong, Colloids Surf. B **65**, 18 (2008).
[11] J.H. Wang, X.J. Han, H.R. Ma, Y.F. Ji, L.J. Bi, Chem. Eng. J. **173**, 171 (2011).
[12] K.L. Jarvis, P. Majewski, J. Colloid Interface Sci. **380**, 150 (2012).
[13] S. Han, S. Kim, H. Lim, W. Choi, H. Park, J. Yoon, T. Hyeon, Micropor. Mesopor. Mat. **58**, 131 (2003).
[14] A. Imyim, E. Prapalimrungsi, J. Hazard. Mater. **184**, 775 (2010).
[15] J.N. Wang, Y. Zhou, A.M. Li, L. Xu, J. Hazard. Mater. **176**, 1018 (2010).
[16] A. Radian, M. Carmeli, D. Zadaka-Amir, S. Nir, E. Wakshal, Y.G. Mishael, Appl. Clay Sci. **54**, 258 (2011).
[17] M.S. Wang, L.B. Liao, X.L. Zhang, Z.H. Li, Appl. Clay Sci. **67-68**, 164 (2012).
[18] Y.L. Tang, S. Liang, S.L. Yu, N.Y. Gao, J. Zhang, H.C. Guo, Y.L. Wang, Colloid Surf. A **406**, 61 (2012).
[19] A. Negrulescu, V. Patrulea, M. mincea, C. Moraru, V. Ostafe, Digest J. Nanomat. Biostruct. **9**, 45 (2014).
[20] Y.H. Zhan, J.W. Lin, J. Li, Environ. Sci. Pollut. Res. **20**, 2512 (2013).
[21] Q. Tao, Z.Y. Xu, J.H. Wang, F.L. Liu, H.Q. Wan, S.R. Zheng, Micropor. Mesopor. Mat. **131**, 177 (2010).
[22] G.C. Zhang, T. Wu, Y.J. Li, X.H. Huang, Y. Wang, G.P. Wang, Chem. Eng. J. **191**, 306 (2012).
[23] Z.Z. Zhang, M.Y. Li, W. Chen, S.Z. Zhu, N.N. Liu, L.Y. Zhu, Environ. Pollut. **158**, 514 (2010).
[24] A.B.M., Giasuddin, S.R., Kanel, H. Choi, Environ. Sci. Technol. **41**, 2022 (2007).
[25] H. Esmaeili, A. Ebrahimi, M. Hajian, H.R. Pourzamani, Int. J. Environ. Health Eng. **1**, 33 (2012).
[26] R.X. Wang, T. Wen, X.L. Wu, A.W. Xu, RSC Adv. **4**, 21802 (2014).
[27] C.L. Dong, W. Chen, C. Liu, Appl. Surf. Sci. **292**, 1067 (2014).
[28] K. Yang, D.H. Lin, B.S. Xing, Langmuir **25**, 3571 (2009).
[29] W. Wei, R. Sun, Z.G. Wei, H.Y. Zhao, H.X. Li, F. Hu, J. Liq. Chrom. Rel. Technol. **32**, 106 (2009).
[30] G.M.S. El Shafei, N.A. Moussa, J. Colloid Interface Sci. **238**, 160 (2001).
[31] O. Takagi, N. Kuramoto, M. Ozawa, S. Suzuki, Ceram. Int. **30**, 139 (2004).
[32] I. Mobasherpour, E. Salahi, M. Pazouki, Desalination **266**, 142 (2011).
[33] K.L. Lin, J.Y. Pan, Y.W. Chen, R.M. Cheng, X.C. Xu, J. Hazard. Mater. **161**, 231 (2009).
[34] J. Beuvelot, Y. Mauras, G. Mabilleau, H. Marchand-Libouban, D. Chappard, Digest J. Nanomat. Biostruct. **8**, 207 (2013).
[35] A. Sobczak-Kupiec, D. Malina, B. Tyliszczak, M. Piątkowski, K. Bialik-Wąs, Z. Wzorek, Digest J. Nanomat. Biostruct. **7**, 459 (2012).
[36] W. Wei, X. Zhang, J. Cui, Z.G. Wei, J. Liq. Chrom. Rel. Technol. **33**, 1335 (2010).
[37] Y. Wang, N.P. Chen, W. Wei, J. Cui, Z.G. Wei, Desalination **276**, 161 (2011).
[38] I. Smičiklas, A. Onjia, S. Raičević, Sep. Purif. Technol. **44**, 97 (2005).
[39] B. Tang, L. Yuan, T. Shi, L. Yu, Y. Zhu, J. Hazard. Mater. **163**, (2009) 1173-1178.
[40] L.Y. Cao, C.B. Zhang, J.F. Huang, Ceram. Int. **31**, 1041 (2005).
[41] Z. Chen, Y. Zhou, Z. Kang, D. Chen, J. Alloys Comp. **609**, 21 (2014).
[42] I.D. Smičiklas, S.K. Milonjić, P. Pfendt, S. Raičević, Separ. Purifi. Technol. **18**, 185 (2000).
[43] S. Lagergren, Zur theorie der sogenannten adsorption gelöster stoffe, K. Sven. Vetenskapsakad. Handl, Band **24**, 1 (1898).

[44] Y.S. Ho, G. McKay, Process Biochem. **34**, 451 (1999).
[45] I. Langmuir, J. Am. Chem. Soc. **40**, 1361 (1916).
[46] H.M.F. Freundlich, Z. Phys. Chem. **57**, 385 (1906).
[47] R. Sips, J. Chem. Phys. **16**, 490 (1948).
[48] C. Stötzel, F.A. Müller, F. Reinert, F. Niederdraenk, J.E. Barralet, U. Gbureck, Colloids Surf. B **74**, 91 (2009).
[49] M. Darroudi, H. Eshtiagh-Hosseini, M.R. Housaindokht, Digest J. Nanomat. Biostruct. **5**, 29 (2010).
[50] N.C.C. Da Rocha, R.C. De Campos, A.M. Rossi, E.L. Moreira, A. Do. F. Barbosa, G.T. Moure, Environ. Sci. Technol. **36**, 1630 (2002).
[51] S. Gao, R. Sun, Z.G. Wei, H.Y. Zhao, H.X. Li, F. Hu, J. Fluorine Chem. **130**, 550 (2009).
[52] L.M. Wu, W. Forsling, P.W. Schindler, J. Colloid Interface Sci. **147**, 178 (1991).
[53] I. Smičiklas, S. Dimović, I. Plećaš, M. Mitrić, Water Res. **40**, 2267 (2006).
[54] H. Bouyarmane, S.E. Asri, A. Rami, C. Roux, M.A. Mahly, A. Saoiabi, T. Coradinc, A. Laghzizil, J. Hazard. Mater. **181**, 736 (2010).
[55] W. Wei, X. Zhang, J. Cui, Z.G. Wei, Colloids Surf. A **392**, 67 (2011).
[56] B. Vlad-oros, D. Dascalu, Z. Dudas, H. Popovici, G. Preda, V. Ostafe, Digest J. Nanomat. Biostruct. **8**, 917 (2013).
[57] J.H. Wang, L.J. Bi, Y.F. Ji, H.R. Ma, X.L. Yin, J. Colloid Interface Sci. **430**, 140 (2014).
[58] S.B. Wang, Z.H. Zhu, J. Colloid Interface Sci. **315**, 41 (2007).
[59] A.W.P. Vermeer, W.H. Van Riemsdijk, L.K. Koopal, Langmuir **14**, 2810 (1998).
[60] X.J. Peng, Z.K. Luan, F.T. Chen, B.H. Tian, Z.P. Jia, Desalination **174**, 135 (2005).
[61] D. Doulia, Ch. Leodopoulos, K. Gimouhopoulos, F. Rigas, J. Colloid Interface Sci. **340**, 131 (2009).
[62] M. Erhayem, M. Sohn, Sci. Total Environ. **468**, 249 (2014).
[63] S. Zhang, Hydroxyapatite Coatings for Biomedical Applications, CRC, Press, BocaRaton, FL, 2013.
[64] A.B.H. Yoruc, Y. Koca, Digest J. Nanomat. Biostruct. **4**, 73 (2009).
[65] M. Brigante, G. Zanini, M. Avena, J. Hazard. Mater. **184**, 241 (2010).
[66] J. Zhang, J.L. Dai, R.Q. Wang, F.S. Li, W.X. Wang, Colloid Surf. A **335**, 194 (2009).
[67] C. Rivero, N. Senesi, J. Paolini, V. D'Orazio, Geoderma **81**, 227 (1998).
[68] T.S. Anirudhan, P.S. Suchithra, S. Rijith, Colloid Surf. A **326**, 147 (2008).
[69] T. Moriguchi, K. Yano, S. Nakagawa, F. Kaji, J. Colloid Interface Sci. **260**, 19 (2003).